

SINGLE-SPECIES WEIBEL INSTABILITY OF RADIATIONLESS PLASMA

L. V. Borodachev^a, D. O. Kolomiets^b

Department of Mathematics, Faculty of Physics,
M.V. Lomonosov Moscow State University, Moscow 119991, Russia.

E-mail: ^aborodach2000@mail.ru, ^bkolomiets@darwincode.org

Draft // Sept. 2009

Abstract. A Particle-in-Cell (PIC) numerical simulation of the electron Weibel instability is applied in a frame of Darwin (radiationless) approximation of the self-consistent fields of sparse plasma. As a result, we were able to supplement the classical picture of the instability and, in particular, to obtain the dependency of the basic characteristics (the time of development and the maximum field energy) of the thermal anisotropy parameter, to trace the dynamic restructuring of current filaments accompanying the nonlinear stage of the instability and to trace in detail the evolution of the initial anisotropy of the electron component of plasma.

Keywords: Weibel instability, Particle-in-Cell, PIC, Vlasov–Darwin model.

PACS: 44.05.+e – Direct numerical simulations; 78.20.Bh – Theory, models, and numerical simulation; 29.27.Bd – Beam dynamics, collective effects and instabilities; 52.35.-g – Waves, oscillations, and instabilities in plasmas and intense beams.

Introduction

As it is well known, anisotropic distribution of thermal velocities in homogeneous collisionless plasma may lead to Weibel instability (WI) in case of spontaneous generation of transverse to direction of anisotropy magnetic field [1]. The peculiarity of WI is to have a regime where unstable growth of magnetic field generated by arisen current layers (filaments in multidimensional case) is followed by dynamic transformation of the current structures and stabilization of the magnetic field energy after saturation of the instability.

The general picture of Weibel instability mentioned above has significant variations in several of practically important applications of plasma physics, e.g. WI in relativistic plasma which absorbed high-energy EM impulse [2] is considerably different comparing to WI occurring in the current sheet of Earth’s magnetotail [3], which in turn differs from WI of intense ion beams [4]. That variety of forms along with fundamental nature of WI stimulate its further study using different approaches, one of which is a PIC-method based on Vlasov–Darwin model [5] applied below. Presence of well-developed linear theory of electromagnetic insta-

bilities [6], a typical representative of which is WI, allows one to verify the obtained numerical results.

This work is devoted to the numerical simulation of the electron Weibel instability in order to clarify its general picture, in particular, the evolution of the initial anisotropy on the time, and the dependency of key instability characteristics of the initial anisotropy. Ions due to inertia are considered to be a neutralizing positive background.

1 Elements of linear theory of Weibel instability

Here we review basic results of the linear theory applied to Weibel instability in its most simple, 1D3V (x, v_x, v_y, v_z), setup.

Let’s consider a homogeneous collisionless plasma with a positive (ion) background and anisotropic distribution of thermal velocities of electrons, given by the following distribution function:

$$f_0(\vec{v}) = \frac{n_0 \exp\left(-\frac{v_x^2}{u_x^2} - \frac{v_y^2}{u_y^2} - \frac{v_z^2}{u_z^2}\right)}{\pi^{3/2} u_x u_y u_z} \quad (1)$$

where n_0 is the density of electrons, u_x, u_y, u_z are the thermal velocities of the electrons along the corresponding axes, where we assume (without loss of generality) $u_z > u_x = u_y$.

In this case the plasma, obviously, has an excess of fast particles moving along z -axis. However, due to the symmetry of the distribution, the total current is zero.

Now assume that there exists spontaneously generated (due to thermal fluctuations) non-zero magnetic field $\vec{B}_0 = \vec{e}_y B_{y0} \sin(k_x x)$. Then the Lorentz force $\vec{F}_L = -e\vec{v} \times \vec{B}_0/c$ will change the trajectory of a particle moving along z , which will lead to formation of spatially separated current sheets. Localization of these sheets will coincide with the zeros of the magnetic field which caused the deflection of the particles. Thus, we should expect formation of two current sheets (with opposite signs) per each wavelength of the magnetic field perturbation, amplifying the initial magnetic field. The growth of the field, which in turn increases density of the current sheets, will continue until the major part of the particles become significantly magnetized. Fig. 1 shows a qualitative illustration of this process.

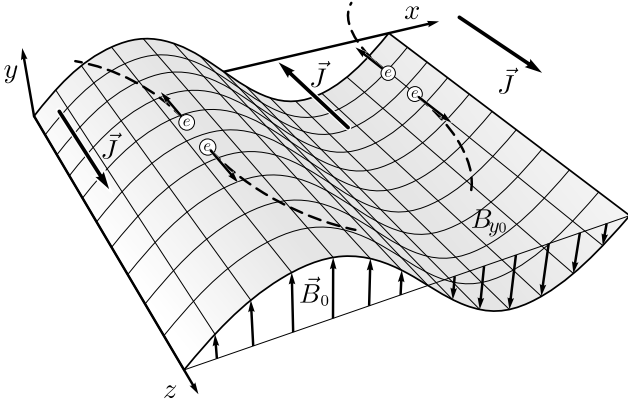


Fig. 1. Qualitative representation of the linear phase of Weibel instability. Development of current sheets \vec{J} around the zeros of B_y (shown as a surface). B_x, B_z considered zero for simplicity

In the described setup the perturbed quantities are $E_z(x, t)$, $B_y(x, t)$ (unperturbed values of which are zero) and the electron distribution function $f(x, \vec{v}, t) = f_0(\vec{v}) + f_1(x, \vec{v}, t)$.

Let the perturbations (as it's common for linear analysis in general) to be represented as $\exp(i(k_x x - \omega t))$. Then, substituting the corresponding values into the Vlasov equation and the field equations, we obtain (as it is shown in [7]) a dispersion equation

$$k_x^2 c^2 - \omega^2 = \omega_{pe}^2 \left(A + \frac{\omega(A+1)}{k_x u_x} Z\left(\frac{\omega}{k_x u_x}\right) \right), \quad (2)$$

where $\omega_{pe} = \sqrt{4\pi n_0 e^2/m}$ is the electron plasma frequency, $A = (u_z^2/u_x^2 - 1)$ is the anisotropy parameter and Z is the plasma dispersion function [8]:

$$Z(\zeta) = \frac{1}{\sqrt{\pi}} \int_{-\infty}^{\infty} \frac{e^{-s^2}}{s - \zeta} ds.$$

where ζ in general is a complex value.

The unstable roots of Eq. (2) (solutions with purely imaginary positive ω , the standing waves) are in the range from $kc/\omega_{pe} = 0$ to $kc/\omega_{pe} = \sqrt{A}$ for any $A > 0$. Thus in the case when the dimensionless wave number k_x falls into this interval, there is a sharp increase in the amplitude of the perturbation of the corresponding wavelength, which is a key feature of the initial stage of WI. The growth rate $\gamma = i\omega$ has a single maximum in the above-mentioned range, which allows to determine the most unstable mode. Note that it's hard (if at all possible) to get analytical solution of this equation, but it is rather easy to solve it numerically with any standard method [9]. The foregoing is illustrated in Fig. 2 where the graphs of the growth rate are shown for various values of anisotropy parameter with fixed accentuated (u_z) thermal velocity.

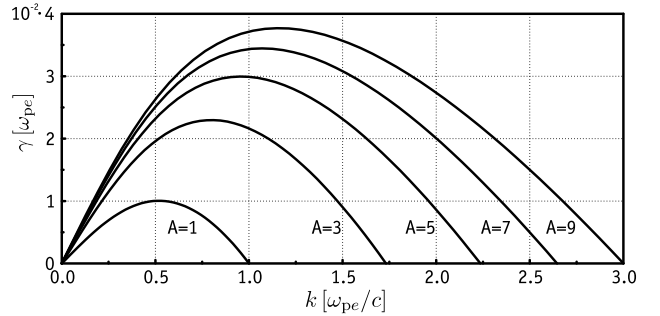


Fig. 2. Growth rate of WI for various values of anisotropy at constant accentuated thermal velocity $u_z = 0.1 [c]$

2 Numerical simulations

Here we briefly review the results of the numerical simulation of WI in 2.5-dimensional (x, y, v_x, v_y, v_z) setup, where accentuated component of the thermal velocity is taken perpendicularly to the simulation plane x - y . Note that in this case the development of the instability will now be supported with formation of current filaments (beams), rather than layers, as it was in 1.5-dimensions. However, the results of the linear theory presented above are still valid in this case, if one assumes $k_x = k_y = k$.

Then, we specify the uniform spatial distribution of electrons and singly charged ions, the latter ones are

considered as a motionless neutralizing background. In the expression (1) we choose $u_z = 0.1 [c]$, $u_x = u_y = 0.0316 [c]$. For these values of thermal velocities the anisotropy parameter equals to $A_0 = 9$. Note that in the following series of experiments the variation of the anisotropy parameter A_0 carried out by varying of $u_{x,y}$ with fixed $u_z = 0.1 [c]$.

The minimal linear size of the computational domain, which we can choose for the simulation, must correspond to the wavelength for which the dispersion equation (for given values of anisotropy and accentuated thermal velocity) shows the instability growth rate close to maximum (Fig. 2).

In particular, solving numerically the equation (2) for $A_0 = 9$ and $u_z = 0.1 [c]$, we obtain the approximate value of $\gamma_{\max} = 0.037$ and the corresponding value of $k_{\max} = 1.2 [\omega_{pe}/c]$, in terms of the wavelength it will give us $\lambda_{\max} = 5.2 [c/\omega_{pe}]$.

Thus choosing $L_x = 25 [c/\omega_{pe}]$, $L_y = 25 [c/\omega_{pe}]$ will allow us to trace in detail the development of initial current system and its restructuring in nonlinear stage of WI.

Finally, following the work [7], we choose periodic boundary conditions for both x and y directions.

The instability development process is clearly visible on the plots of the average over space magnetic field energy density versus time for different initial values of the anisotropy shown in Fig. 3.

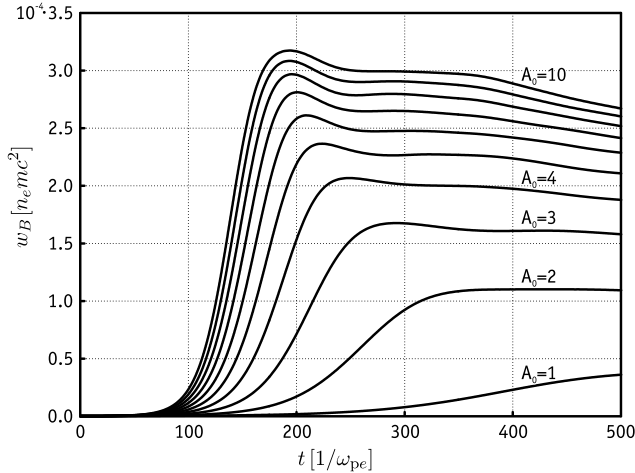


Fig. 3. Average magnetic field energy density versus time for different values of initial anisotropy ($A_0 = 1...10$) at constant accentuated thermal velocity. Computational domain $L_x = L_y = 25 [c/\omega_{pe}]$; $u_z = 0.1 [c]$; mesh size 128×128 ; 500 particles of each specie per cell; time step $\tau = 0.25 [1/\omega_{pe}]$

The initial value of the average energy density is close to zero, but by the time $t = 100 [1/\omega_{pe}]$, corresponding to appearing of distinguishable areas of current localization, it is observed a noticeable increase, which is

the greater the larger is the initial anisotropy of the plasma. As noted above, the linear stage ends when the system formed a pronounced current structure consisting of a system of current beams (Fig. 6, time slice $t = 150 [1/\omega_{pe}]$), and when the particles become significantly magnetized in average (mean Larmor radius is of the order of the current beam radius).

Further development of the WI is nonlinear and is accompanied by dynamic merging of equidirected current filaments into larger-scale structures, that can be seen from a series of time slices shown in Fig. 6. Along with that the magnitude of the magnetic field energy stabilizes. Note that the merging continues until the velocity distribution of the electrons does not become an equilibrium.

In that context it is interesting to trace the evolution of the initial anisotropy of the electron component during the development of WI, including at the non-linear stage. The dependence of the anisotropy on the time is shown in Fig. 4. From the figure one can see that the process of growth and further stabilization of current density and magnetic field energy density is accompanied by isotropization (decrease in the anisotropy) of the medium, caused by collective processes of formation and restructuring of current filaments together with competitive development of the unstable modes of the magnetic field.

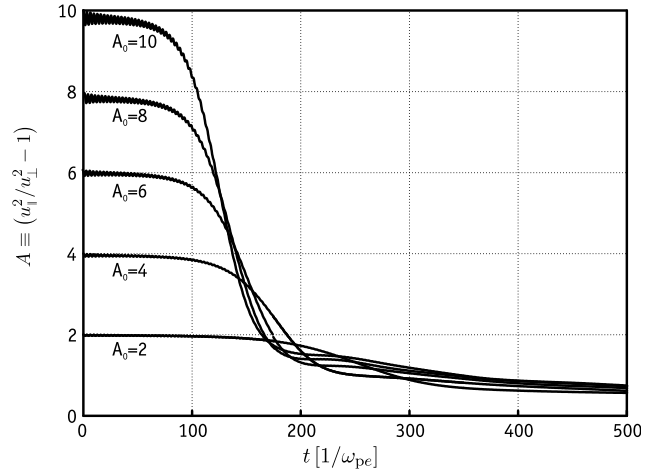


Fig. 4. Evolution of the anisotropy for different initial A_0 . The same setup as for Fig. 3

It is interesting to note here an non-obvious fact that regardless of the initial value of the the anisotropy, its value at the instability saturation stage tends to a nonzero threshold value (see Fig. 4).

The origin for that residual anisotropy is in the problem setup, and it is connected with an actual finiteness of the perturbation spectrum of any system with periodic boundary conditions, due to the fact that

in such a system waves longer than linear size of the domain can not exist.

This conclusion is confirmed by the results of [10], where it is shown that for a limited system (in the sense stated above) the minimum level of the anisotropy at the saturation stage of WI can be defined by the following expression:

$$A_{\min} = (k_{\min}c/\omega_{pe})^2,$$

In our case the minimal wave number allowed in the system is $k_{\min}c/\omega_{pe} = 2\pi/L_{x,y} = 2\pi/25 = 0.25$, which gives $A_{\min} = 0.063$. Some discrepancy of the experimentally observed levels of residual anisotropy (Fig. 4) and its theoretically predicted value can be explained by the fact, that at time $t = 500 [1/\omega_{pe}]$ the dominant mode of the instability has not yet reached the limit determined by the period of the system. As stated above, one of the objectives of these experiments was to clarify the dependence of the basic characteristics of the instability—its growth rate, the characteristic time and the maximum energy density of the magnetic field, of the initial anisotropy of plasma.

In this connection let's return to Fig. 3, from which one can see the expected effect: the increase of the maximum field energy density and instability growth rate with the increase of initial anisotropy. Less trivial is the profile of this dependency shown in Fig. 5: fast increase of the maximum energy density on the interval $A_0 < 10$, followed by an equally fast drop-off with $A_0 > 10$.

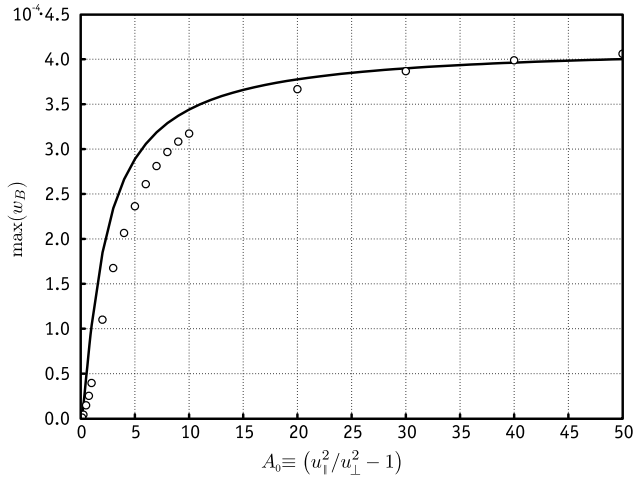


Fig. 5. The dependency of the maximum average magnetic field energy density of the initial anisotropy at constant accentuated thermal velocity $u_z = 0.1 [c]$. The same setup as for Fig. 3

Moreover the value of A_0 around 25 can be considered as an upper threshold of instability in the sense that further increase in the initial anisotropy of electron

component has virtually no effect on the basic characteristics of the WI—the maximum value of magnetic field energy density (in case of fixed value of accentuated thermal velocity u_z). The observed effect and its quantitative characteristics are confirmed by analytical expression which can be obtained on the basis of the expression derived in the work [10]:

$$\frac{w_B}{n_0 T_{z0}} = \frac{1}{3} \left(\frac{A}{A+1} \right) \left(\frac{1}{A+1} - \frac{1}{A_0+1} \right), \quad (3)$$

where T_z is the temperature of accentuated electron component along z -axis.

In the just mentioned work the expression (3) has been used as an estimation of evolution of the magnetic field energy density, where the values of A were being taken from the numerical simulation.

However, in our context, it can be interpreted as an analytical dependence of the magnetic field energy density (in units of $n_0 T_z$) of the current value of anisotropy A with its initial value given as A_0 . Considering (3) that way, its easy to get an interesting for us estimation of the maximum energy of WI (or, equivalently, the maximum proportion of the energy of accentuated component which can be converted into field energy) and also the explanation of the existence of upper threshold of WI on A_0 mentioned above. Indeed, differentiating the right hand side of (3) with respect to A and equating the derivative to zero we obtain:

$$\frac{A_0 - A(2 + A_0)}{3(A+1)^2(A_0+1)} = 0.$$

Where from we get the value of the anisotropy coefficient which delivers the maximum to the expression (3) with fixed value of A_0 :

$$A_{\text{extr}} = \frac{A_0}{2 + A_0}.$$

Substituting the resulting value of A_{extr} back into (3), we find the desired dependence of the maximum magnetic field energy on the value of A_0 :

$$w_{B\text{max}} = \frac{n_0 T_{z0} A_0^2}{12(1 + A_0)^2}, \quad (4)$$

Dependency (4) together with the experimental values is shown in Fig. 5. Analysis of the last expression gives a number of interesting provisions which are in good agreement with computer simulation experiments.

First, $w_{B\text{max}}$ has a limit in case of fixed values of n_0 , T_{z0} (u_z) and $A_0 \rightarrow \infty$ (the last one actually means $u_x, u_y \rightarrow 0$)

$$w_{B\text{max}}^{\text{lim}} = \frac{n_0 T_{z0}}{12},$$

corresponding to the maximum possible energy density of WI. Particularly, in our case, where $n_0 T_{z0} = 0.005 [n_e mc^2]$, $w_{B\text{max}}^{\text{lim}}$ equals to $4.1 \cdot 10^{-4} [n_e mc^2]$,

which, as it can be seen in Fig. 5, is in good agreement with the numerical data.

Second, observed in experiments, the upper threshold of WI with respect to A_0 is determined by the value of A_0 , from which the fraction $A_0^2/(1 + A_0)^2$ becomes close to unity. It is easy to see that the value of A_0 close to 25 meets this requirement (indeed, if $A_0 = 25$ the fraction equals to 0.925, and if $A_0 = 50$, i.e. increased by factor of two, it only slightly increases up to 0.96).

Third, the portion of energy stored in the accreted component of the system which goes for development of Weibel instability depends on the degree of the initial anisotropy (A_0) and it can not be higher than 1/12. For instance, in our experiments it varies from 6.2% (for $A_0 = 9$) down to 2.2% (for $A_0 = 2$). These data are consistent both with the analytical predictions obtained from the expression (4) and with the upper limit of the converted anisotropy energy (around 10%) obtained in [7], where 2D simulation has been performed in the frame of full electromagnetic model of plasma.

Note also that if we define the characteristic time of the instability (T_I) as the time needed to reach the maximum of magnetic field energy density, then from the same Fig. 3 one can easily estimate the dependency of the characteristic time T_I of the initial anisotropy A_0 .

We also note good agreement between the numerical values of the dimensionless instability growth rate

(0.034) with the ones predicted by the linear theory (0.037) for the setup considered above where $A_0 = 9$ and $u_z = 0.1 [c]$.

Conclusion

Thus, the performed computer experiments allowed to supplement the classical picture of the Weibel instability. Particularly, we obtained the dependency of the characteristic time of its development and the maximum magnetic field energy density of the initial value of the anisotropy parameter. Also we have traced the dynamic restructuring of the current filaments accompanying nonlinear stage of instability saturation, as well as the evolution of the initial anisotropy of the electron component of the plasma.

As a further work it is planned to perform a numerical study of the dynamics and generation mechanisms of two-species Weibel instability, which implies a kinetic representation not only of electron but also ion plasma components in the time scale by orders of magnitude greater than it is for a single-species WI.

Acknowledgments

The authors consider it their pleasant duty to thank Acad. L. M. Zelenyi and Dr. H. V. Malova from Russian Space Research Institute for numerous constructive discussions of the results presented in this work.

References

- [1] *Weibel E. S.* Spontaneously Growing Transverse Waves in a Plasma Due to an Anisotropic Velocity Distribution. // Phys. Rev. Lett., v. **2**, 1959, 83–84.
- [2] *Pukhov A., Meyer-ter-Vehn J.* Relativistic Magnetic Self-Channeling of Light in Near-Critical Plasma: Three-Dimensional Particle-in-Cell Simulation. // Phys. Rev. Lett., v. **76**, №21, 1996, 3975–3978.
- [3] *Yoon P. H., Lui A. T. Y.* Nonlocal ion-Weibel instability in the geomagnetic tail. // J. Geophys. Res., v. **101**, №A3, 1996, 4899–4906.
- [4] *Davidson R. C., Startsev E. A., Kaganovich I., Qin H.* Multispecies Weibel Instability for Intense Ion Beam Propagation Through Background Plasma. // PAC 2005. Proceedings, 2005, 1952–1954.
- [5] *Borodachev L. V., Mingalev I. V., Mingalev O. V.* Vlasov–Darwin System. // Encyclopedia of Low Temperature Plasma (Series B), v. **VII**. M.: "Janus-K", 2008, 136–146.
- [6] *Mikhailovsky A. B.* Theory of Plasma Instabilities. M.: Atom Press, 1975.
- [7] *Morse R. L., Nielson C. W.* Numerical Simulation of the Weibel Instability in One and Two Dimensions. // The Physics of Fluids, v. **14**, No. 11, 1971, 830–840.
- [8] *Frank-Kamenetskii D. A.* Lectures on plasma physics. M.: Atom Press, 1964.
- [9] *Kalitkin N. N.* Numerical Methods. M.: "Nauka", 1978.
- [10] *Lemons D. S., Winske D., Gary S. P.* Nonlinear theory of the Weibel instability. // J. Plasma Phys., v. **21**, part 2, 1979, 287–300.

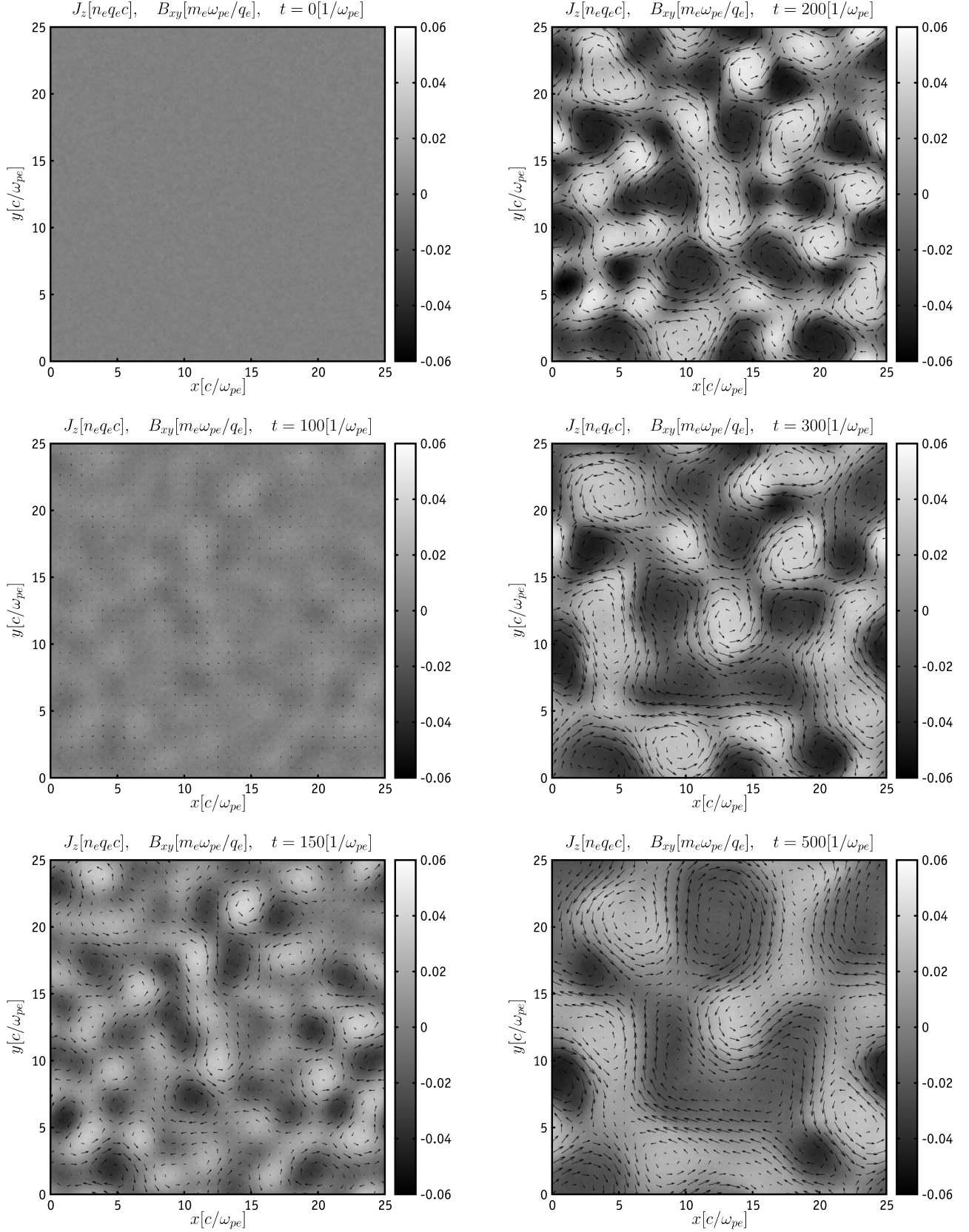


Fig. 6. The current density J_z and the magnetic field B_{xy} at different time moments for 2.5-dimensional setup of WI in case $A_0 = 9$. Computational domain $L_x = L_y = 25$ [c/ω_{pe}]; $u_z = 0.1$ [c]; mesh size 256×256 ; 1000 particles of each specie per cell; time step $\tau = 0.25$ [$1/\omega_{pe}$]